Control of Dynamic Stall in a H-Darrieus VAWT Using Blade Leading Edge Protuberances

Afonso Dias Nogueira Capelo Gonçalves
afonso.nogueira@tecnico.ulisboa.pt

Instituto Superior Técnico, Universidade de Lisboa, Portugal

December 2021

Abstract

Dynamic stall flow conditions affect the performance of most Vertical Axis Wind Turbine (VAWT) designs; however, the associated losses are especially relevant in smaller turbines, such as those typically used in urban environment applications. The work described in this dissertation experimentally evaluated the efficacy of leading edge protuberances in controlling the aforementioned stall behaviour.

A numerical study was first performed to define the leading edge geometry to be subsequently tested in the wind tunnel. A custom experimental setup was also developed for this purpose.

The wind tunnel measurements of the modified turbine showed significant performance gains over the baseline and a considerably improved self-starting behaviour. The power coefficient increase was between 46% and 20% for wind speeds ranging from 5.5 m/s to 9 m/s. The tip speed ratio behaviour of the studied turbine was not meaningfully affected by the leading edge protuberances.

Keywords: Vertical axis wind turbine, dynamic stall, experimental study, computational fluid dynamics, leading edge protuberances, vortex generators

1. Introduction

Horizontal Axis Wind Turbines (HAWT) have long been established as the best turbine configuration for large scale onshore and offshore wind power production. For smaller scale power generation, however, the advantages offered by lift type Vertical Axis Wind Turbine (VAWT) designs can outweigh the disadvantages that typically make them less ideal in larger scale scenarios.

These advantages range from an intrinsic insensitivity to wind direction and lower noise production to an overall better performance under turbulent and skewed flow conditions [1], which makes VAWTs especially appropriate to urban areas [2] and, in general, environments with transient and unsteady wind characteristics [3].

Nevertheless, complex rotor aerodynamics due to constantly changing angles of attack and poor self-starting behaviour are still characteristic of VAWT designs, which contribute to an altogether typically lower efficiency, particularly in smaller turbines and at lower blade speeds.

The main contributing factor for this decrease in performance are the dynamic stall conditions that the rotors are typically subjected to. Dynamic stall normally occurs at tip speed ratios $\lambda < 5$ [4], precisely as a result of the oscillating nature of the flow over the blades' surfaces. Fig. 1 displays the amplitude of the angle of attack fluctuations as function of the λ.

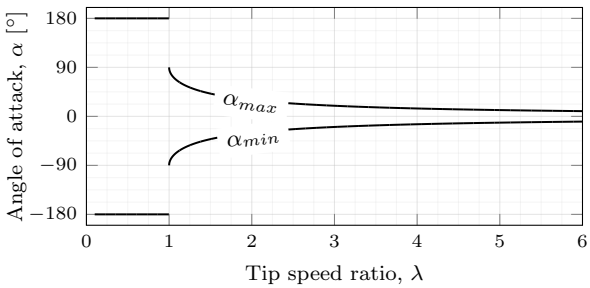

Figure 1: Maximum and minimum angle of attack as a function of λ.

At low λ , the effective angle of attack exceeds the static stall angle of the airfoil, α_{ss} (measured to be around $\alpha_{ss} = \pm 10.5°$ for a NACA0018 airfoil at $Re = 3.8 \times 10^4$ [4]), in considerable portions of the rotation cycle.

This behaviour will naturally degrade the power output and start up capabilities of the turbine, resulting in overall lower efficiency.

In large vertical axis turbines the dynamic stall effects can be mitigated by increasing the operational tip speed ratio. In turn, the same can only be accomplished in rotors with small diameters by increasing the rotational speed, Ω, see Eq. (1).

$$\lambda = \frac{\Omega R}{U_\infty}. \tag{1}$$

However, whereas the centripetal force, F_c, applied to each blade is proportional to the rotor diameter, Eq. (1), it scales with the square of the rotational speed, Eq. (2).

As such, improving turbine performance under dynamic stall is especially relevant to small scale VAWT power generation, seeing how higher tip speed regimes are only achievable with impractical structural loads.

$$F_c = \frac{mV^2}{R} = m\Omega^2 R \tag{2}$$

1.1. State of the art

Several active flow control methods have been proposed with the objective of improving the stall behaviour of wings/blades, namely, boundary layer blowing and suction [5] [6], pulsed vortex generator jets [7], and synchronous variable pitch blades [8].

Passive flow control techniques have also been studied with the same propose. The associated simplicity in comparison with active methods is of special advantage in small turbine applications.

Joo et al. [9] employed a nose droop and a Gurney flap to a rotor airfoil (NACA0012) and showed an improvement in the aerodynamic forces generated in dynamical stall conditions. Carr et al. [10] also obtained promising results by using fixed slats.

Vortex generators have also been studied and used in many fields as a way to suppress or delay separation in quasi-static conditions [11]. Concerning wind turbines, Zhu et al. [12] [13] and Tavernier et al. [14], analysed the effects of more traditional vortex generators on a oscillating airfoil (commonly used in wind turbines). The authors reported an effective delay of dynamic stall and an increase in the maximum C_L.

Recently, leading edge vortex generators inspired by the protuberances of humpback whales' flippers have prompted several research studies, e.g., [15]–[17]. This leading edge modification has been shown to trigger the formation of two counter rotating vortices between each protuberance that can potentially improve the stall performance of the airfoil [18]–[20].

Johari et al. [21] tested several sinusoidal leading edge geometries on an airfoil at $Re = 1.83 \times 10^5$. The water tunnel tests showed an overall different stall behaviour for the modified airfoils. The protuberances degraded slightly the pre-stall performance but increased the lift coefficients after the critical stall angle of the baseline airfoil and displayed overall smoother lift curves. Furthermore, the results from [21] also show that the amplitude of the sine wave that defines the leading edge shape plays a larger role in the airfoil's behaviour than the wavelength.

Guerreiro and Sousa [19] also studied these sinusoidal leading edges in the wind tunnel at lower Reynolds numbers ($Re = 7.0 \times 10^4 - 1.4 \times 10^5$) and for different aspect ratios. The authors reported similar improvements to the stall regime of the airfoils, especially at $Re = 7.0 \times 10^4$ and for the wing with the larger aspect ratio, in which the influence of the wingtip vortices was less significant. These results further reinforce the utility of this leading edge morphology to wings operating in the stall regime.

The numerical study by Câmara and Sousa [18] showed similar results using Detached Eddy Simulations (DES) and further elucidated the streamwise vortices structure.

Concerning the application of this technology in VAWTs, multiple numerical studies have been published. Wang and Zhuang [22] analysed the performance of leading edges protuberances (serrations) in a small two bladed H-Darrieus turbine, operating at $\lambda < 4$. The 3D unsteady RANS simulations, using the realizable $k-\epsilon$ turbulence model, showed a promising increase in power output (between 50% and 15%) throughout the whole tip speed ratio and wind speed range. This for the best leading edge geometry analysed: $\lambda_{vg} = 1/3c$; $A_{vg} = 0.025c$.

The subsequent numerical study by Wang et al. [23] described the optimisation of a three bladed VAWT with similar overall dimensions and solidity and the influence of twist angle (helical rotor) was also accounted for. For both the helical and straight blade rotor configurations, the best leading edge geometry was equivalent to the one proposed in [22], but with half of the wavelength (i.e., $\lambda_{vg} = 1/6c$; $A_{vg} = 0.025c$).

Another article, by Yan et al. [24], points to better performance, for a higher solidity VAWT, with a more conservative leading edge geometry: $\lambda_{vg} = 0.4c$; $A_{vg} = 0.01c$.

Additionally, the start-up behaviour improvements provided by leading edge protuberances was experimentally investigated by Du [25].

Further possible improvements of a VAWT's efficiency under nominal operation through the use of leading edge protuberances have yet, to the author's knowledge, to be experimentally tested.

Therefore, the main objective of this study was

to experimentally investigate the efficacy of leading edge protuberances vortex generators in reducing the dynamic stall effects and thus increasing the efficiency of a small scale vertical axis wind turbine.

2. Methodology

2.1. Turbine design

The design of the baseline turbine model was mainly constrained by the wind tunnel's test area dimensions—i.e., 800 mm (height) × 1350 mm (width).

The final dimensions and parameters are displayed in table 1. The main objective of the baseline turbine design was to ensure that it is reasonably optimised, and that the results from this study are also applicable to the more common small and medium scale Darrieus wind turbine designs.

Table 1: Turbine final dimensions.

H-Darrieus rotor	
Number of blades - N	3
Height / blade span - H	0.45 m
Diameter - D	0.45 m
Chord - c	0.075 m
Airfoil	NACA0018
Swept area - A	0.203 m^2
Rotor aspect ratio - AR	1.0
Solidity - σ	0.5
Blade aspect ratio - AR_b	6.0

2.2. Leading edge protuberances

The geometry of leading edges protuberances is defined by a sinusoidal line with amplitude, A_{vg}, and wavelength, λ_{vg}. To create the protuberances, the profile is stretched or shortened to follow the sinusoidal line at the leading edge. This shape modification is only applied to the front section of the airfoil, in front of the maximum thickness point, Fig. 2.

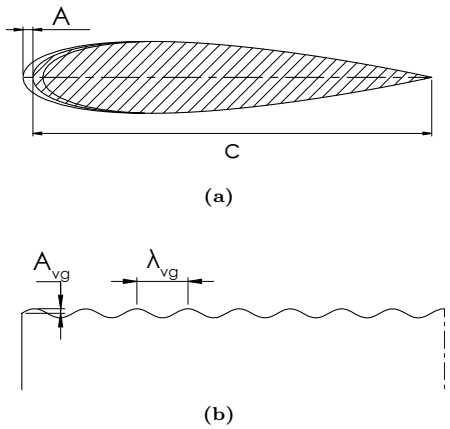

(a)

(b)

Figure 2: Sinusoidal leading edge parameters.

2.3. Numerical method

An infinite blade parametric CFD study was performed in STAR-CCM+ in order to define the best modified leading edge geometry. Finite blade turbine simulations were also carried out, mainly to validate the mesh and numerical models with the wind tunnel data, seeing how it would not be reasonable to directly compare the infinite blade results with the experimental values.

All simulations were performed at $U_\infty = 8\ m/s$, $\Omega = 560\ rpm$ and $\lambda = 1.65$ in order to capture the dynamic stall behaviour of the turbine.

2.3.1 Half-turbine finite blade mesh

The trimmed mesh used in this study was based on the settings employed by Wang et al. [22] [23], given the similarities of the problem.

To simulate the rotational physics of the turbine, a sliding mesh was employed. As such, the domain was split into a stationary (Fig. 3a) and rotating volume (Fig. 3b), interacting through two interfacing surfaces.

Except for the inlet and outlet regions, all boundaries, including the bottom plane, were defined with symmetric boundary conditions.

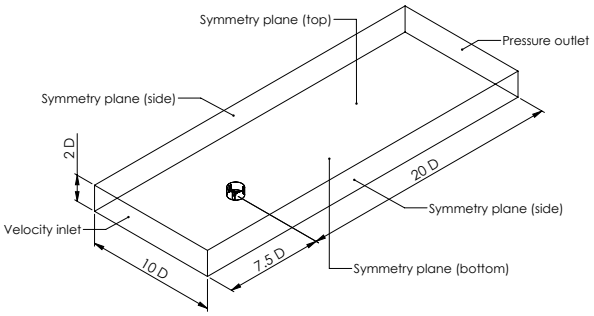

(a) Stationary volume

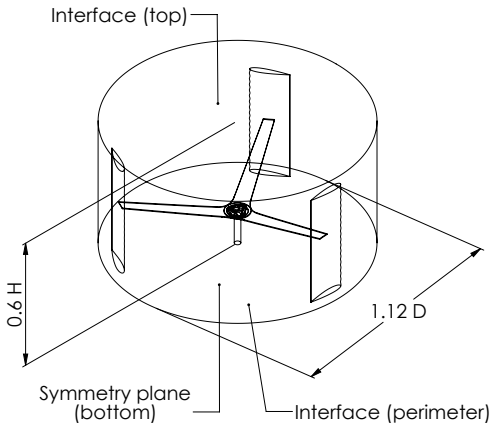

(b) Rotating volume

Figure 3: Finite blade domain.

The mesh refinement in all regions was defined in function of the cell resolution on the blade's surfaces.

The prism layers used over all rotor surfaces were determined both by the y^+ requirements and to provide a smooth transition between the first cell height and the mesh size connected to the last layer.

The mesh refinement around the rotor can be seen in Fig. 4.

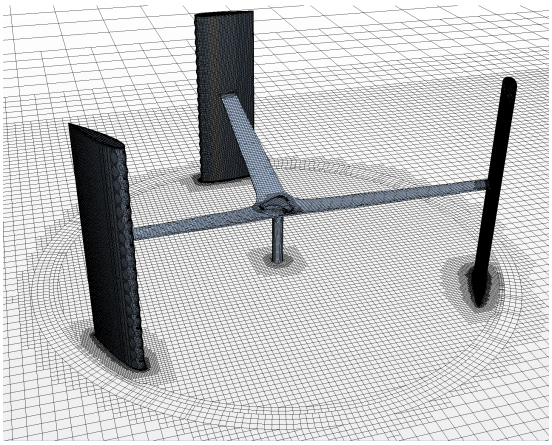

Figure 4: Mesh over rotor surfaces.

2.3.2 Infinite blade mesh

The mesh used in the infinite blade simulations was essentially a slice of the mesh described above, with a height equivalent to two leading edge wavelengths, Fig. 5. This to capture the eventual bi-periodic structure reported in [18] and [24].

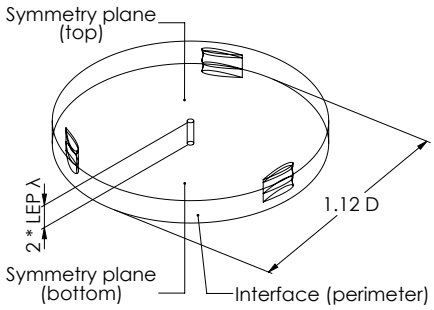

Figure 5: Infinite blade rotating volume.

2.3.3 Solver settings

A segregated flow solver based on the SIMPLE algorithm [26] was used to solve the mass and momentum conservation equations. A second order upwind space discretization scheme was employed to compute the convection moment equation.

Given the dependent nature of the problem, a second order implicit unsteady solver was used to control the time discretization. The time-step was set to the time interval equivalent to an azimuthal increment of $\Delta\theta = 0.5°$, as suggested in [27].

Each simulation was ran until the torque curve stabilised between two consecutive turbine rotations. After the first simulation, to reduce the number of rotations necessary to achieve a converged result, the fields of the previous run were used as initial conditions on the next one.

2.3.4 Mesh resolution, turbulence model and validation with experimental results

Studies like [28] obtained accurate predictions using the $k-\omega$ STT with the $\gamma - Re_{\theta_t}$ transition model but in similar problems, [22] [23], the realizable $k-\epsilon$ model was also employed successfully.

Fig. 6 shows the mesh resolution and turbulence model sensitivity analysis performed. This analysis showed that, in this case, the best performance predictions are obtained using the realizable $k-\epsilon$ turbulence model.

Additionally, given the progressively higher cost of each simulation and the fact that this numerical analysis was only meant to indicate the best leading edge configuration, the convergence shown in Fig. 6 was deemed adequate to establish that increasing the mesh refinement above the resolution defined by a blade surface element with 0.75 mm was not worthwhile.

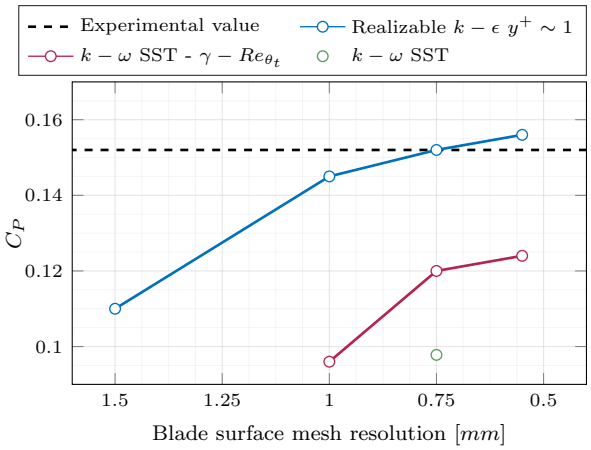

Figure 6: Turbulence models' results comparison.

Table 2 summarises the numerical settings used in these studies.

2.4. Experimental setup

The experimental study was performed in the low-speed wind tunnel of the Mechanical Engineering Department at Instituto Superior Técnico, in a open-jet configuration.

The turbine blades were printed in a Fused Deposition Modelling (FDM) 3D printer, as were the majority of the structural components of the entire setup. The blades were also reinforced with two aluminium spars each. The rest of the rotor structure was made of aluminium and supported by a shaft with a diameter of 12 mm (see Fig. 7).

Table 2: Numerical settings.

Models and solver settings		Mesh and domain settings	
Software	STAR-CMM+	Number of elements (finite/infinite blade)	4.6×10^6/ 3.1×10^5
Turbulence model	two-layer realizable $k-\epsilon$		
Solvers		Boundary conditions	
Flow solver	segregated	Inlet	velocity inlet $U_\infty = 8\ m/s$, $TI = 1\%$
Pressure-velocity coupling	SIMPLE	Outlet	atmospheric pressure outlet
Convection space discretisation	2nd order upwind	Side, top and bottom (midplane)	symmetry condition
Time discretisation	2nd order implicit unsteady	Moving mesh type	sliding mesh
Time-step	$1.488 \times 10^{-4}\ s$	Minimum cell size	$0.75\ mm$
Inner steps	20	y^+ on blade surfaces	~ 1

Figure 7: Turbine assembly.

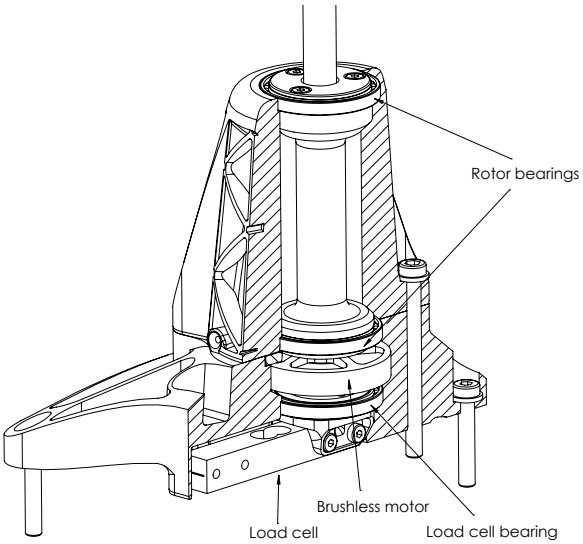

Figure 8: Base assembly.

2.4.1 Torque measurement

In the base assembly, the shaft is connected directly to a brushelss motor used to control the braking torque applied to the turbine. The motor stator is also supported by a bearing and is coupled to a load cell, see Fig. 8.

This way, the turbine torque can be obtained by multiplying the force measured by the load cell with its length (Fig. 9).

The calibration setup of the load cell is described in Fig. 10. A lever arm was clamped around a shaft, coupled directly to the motor rotor, and a known mass was suspended from the tip of the arm through a string and a pulley. This way, a constant known torque could be applied to the load cell while the motor was rotating with a constant speed, simulating the dynamic torque measurement of the turbine's rotor.

The final calibration values are shown in table 3.

Table 3: Final calibration results $[N.mm]$.

Applied torque	Load cell measurements	
	Mean	Error [%]
12.263	12.123	-1.139
20.111	20.416	1.521
30.902	30.765	-0.440
Mean		-0.019

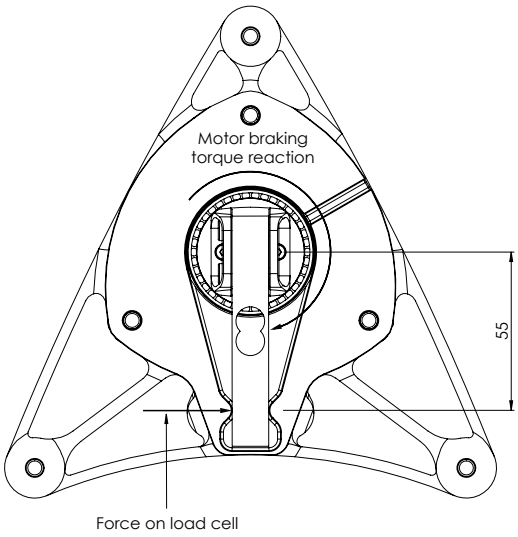

Figure 9: Torque measurement diagram.

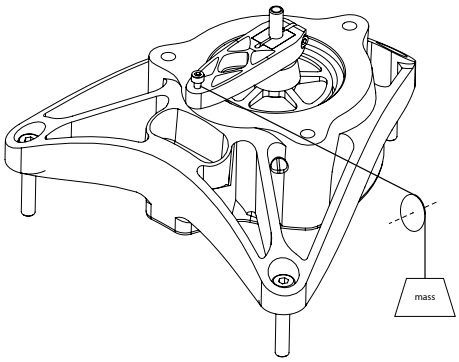

Figure 10: Torque calibration setup.

2.4.2 Rotational speed measurement

The brushless motor used is a small synchronous three phase motor and, as such, rotational speed can be sourced directly from the VESC motor controller in real time.

An optical tachometer was used to validate the rotational speed values measured by the motor controller, at various different speeds, which were found to be within ± 1 rpm of the tachometer values.

2.4.3 Turbine performance

The turbine performance was evaluated through the tip speed ratio, λ, and through the power coefficient, C_P:

$$\lambda = \frac{\Omega R}{U_\infty} \tag{3}$$

$$C_p = \frac{Q\Omega}{\frac{1}{2}\rho U_\infty^3 A} \tag{4}$$

2.5. Uncertainty

Several potential systematic and random error sources were identified throughout the measurement processes of all the variables used to calculate the C_P (Eq. 4). The 95% coverage intervals were determined using a Monte Carlo method, as described in [29], with the standard uncertainties obtained in the validation and calibration processes. The tip speed ratio dependent dispersion observed in different measurements performed in the same conditions, Fig. 11, was also included in the coverage interval.

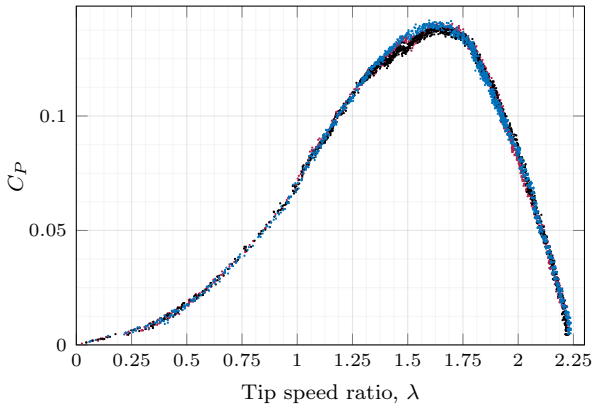

Figure 11: Scatter plot of the three measurements performed at $U_\infty = 7$ m/s in the turbine with the modified leading edge.

2.5.1 Measurement methodology

Every measurement followed the same procedure, resulting in data exemplified in Fig. 12. This process can be summarised by:

1. The turbine rotor is locked and the flow velocity is increased until the desired value.

2. Once the flow velocity stabilises, the rotor is released.

3. In order to evaluate the starting performance of the turbine, no braking torque is applied while the rotational speed increases (apart from the friction torque from the motor, which is registered by the load cell).

4. When the maximum rate of rotation is reached and stabilises, the applied braking torque can be progressively increased until the maximum torque point, after which the torque should be adjusted to allow the rotor to decelerate relatively smoothly. In the first phase, the torque was increased relatively slowly, as to prevent any rotational inertia effects on the measurements.

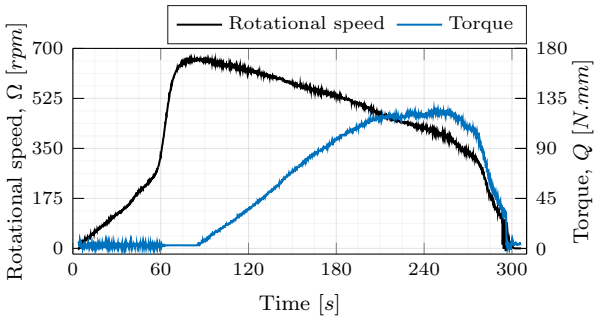

Figure 12: Untreated measured data, $U_\infty = 7\ m/s$.

3. Results and discussion

3.1. Parametric infinite blade CFD study

The performance of each leading edge geometry was compared with the torque coefficient, C_Q, curves and with the power coefficient calculated from the mean torque. C_Q is defined as:

$$C_Q = \frac{Q}{\frac{1}{2}\rho U_\infty^2 A} \tag{5}$$

Since the amplitude of the sinusoidal line that defines the leading edge protuberances was reported in [21], [22], [24] to have a more significant impact on the wing/blade's behaviour than the corresponding wavelength, the first set of simulations was performed with a constant wavelength of $\lambda_{vg} = 1/6c$ and with amplitudes ranging from 3.5% to 0.8% of the chord, c. The corresponding results are compared in Figure 13.

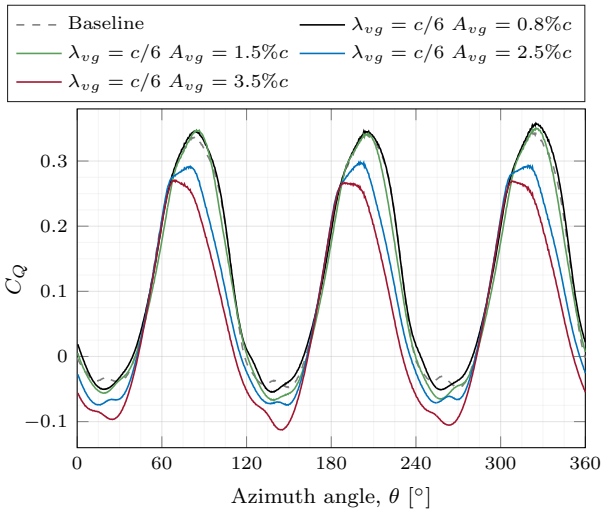

Figure 13: C_Q comparison with different leading edge amplitudes, A_{vg}.

The $A_{vg} = 2.5\%c$ and $A_{vg} = 3.5\%c$ geometries showed a constant decrease in C_Q throughout all rotor positions. The leading edge with $A_{vg} = 1.5\%c$ seems to provide slightly improved torque "peaks" over the baseline curve accompanied, however, by a worse performance in the negative torque regions. The protuberances with an amplitude of $A_{vg} = 0.8\%c$ show similar improvements in the torque "peaks" but also in the negative torque "valleys".

As a result, in the following wavelength analysis, the calculations were carried out with a fixed amplitude of $A_{vg} = 0.8\%c$, which $\lambda_{vg} = 1/6c$ provided a 4% increase in C_P over the baseline

Figure 14 compares the constant amplitude torque curves and substantiates the diminished influence of the leading edge wavelength, especially when compared with the variation shown in the constant wavelength analysis. The only discernible behaviour in this torque curve comparison is between all the modified blades and the baseline; all four modified geometries exhibit higher torque "peaks" and smother "valleys", albeit with increased minimum (negative) torque values.

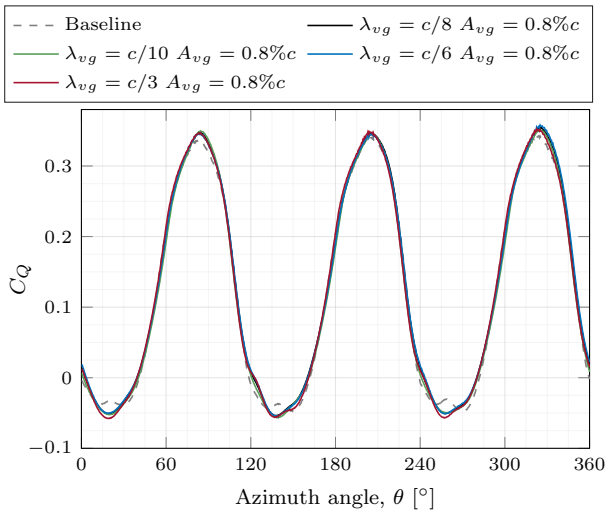

Figure 14: C_Q comparison with different leading edge wavelength, λ_{vg}.

Ultimately, the geometry with a wavelength of $c/6$ and a amplitude equal to 0.8% of the chord, $\boldsymbol{\lambda_{vg} = 1/6c}$; $\boldsymbol{A_{vg} = 0.008c}$, was chosen to be tested experimentally in the modified turbine.

The amplitude of the selected sinusoidal leading edge is significantly more conservative that the values chosen in other studies, for example $\lambda_{vg} = 1/3c$; $A_{vg} = 0.025c$ in [22] and $\lambda_{vg} = 1/6c$; $_{vg} = 0.025c$ in [23], but closer to the value selected in [24]: $A_{vg} = 0.01c$.

Most likely, the relatively small diameter and lower chord Reynolds number favour leading edges with less amplitude.

3.2. Turbine start-up behaviour

The wind tunnel tests revealed that the sensitivity of the self-starting behaviour to the azimuthal blade position remained mostly unchanged between the modified and baseline turbines: they were both able to achieve rotation, without external input, in almost all positions. In a small interval around

$\theta = 40° + n120°$, however, the stationary torque produced by each blade cancelled out and neither turbine was able to initiate operation.

Figure 15 summarises the start-up performance comparison between the baseline and the modified turbine. The significant performance improvement provided by the leading edge vortex generators is evident.

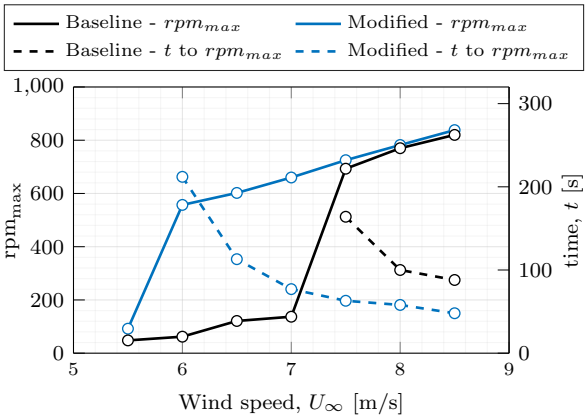

Figure 15: Self-starting performance comparison.

The leading edge protuberances not only improved considerably the wind speed at which the turbine is able to self-start and achieve nominal operation—the modified turbine self-starts at 20% lower wind speeds—but also reduced the time necessary to reach said nominal operation. For the flow conditions where both rotors achieved nominal speeds, $U_\infty = 7.5$ - $8.5\ m/s$, the time to reach λ_{max} was on average 50% smaller.

Even if the efficiency of the turbine had not improved with leading edge vortex generators, this enhancement of the start-up performance alone would still be beneficial to the real-world power output. In varying wind speed environments, faster and earlier start-up equates to less time not producing power once the wind conditions became favourable.

3.3. Turbine performance

The maximum C_P values (table 4) alone show that this leading edge modification significantly improved the efficiency, and consequently, the performance of the turbine throughout the whole analysed range of flow velocities (see also Fig. 17).

As the wind speed increases, the efficiency gain decreases progressively from above 45% to around 20%. This diminishing improvement seems to be, however, a result of a slight increase in performance from the baseline turbine, seeing how much smoother the optimised turbine's C_{Pmax} progression is, especially between $U_\infty = 7\ m/s$ and $U_\infty = 8\ m/s$ (which also coincides with the range were the baseline turbine no longer fails to self-start; Fig. 15).

Additionally, in C_P versus λ curves it is also apparent that the performance improvement is roughly proportional to the C_P in the entire λ range only until $U_\infty = 6.5\ m/s$. Above $U_\infty = 7\ m/s$, the leading edge protuberances only provide a noticeable improvement above $\lambda \sim 1$, like shown in Fig. 16.

Table 4: Maximum power coefficient values.

U_∞	C_{Pmax}	
$[m/s]$	Baseline	$\lambda_{vg} = c/6$; $A_{vg} = 0.8\%c$
5.5	0.0783	0.1141
6.0	0.0878	0.1246
6.5	0.0989	0.1334
7.0	0.1034	0.1384
7.5	0.1093	0.1469
8.0	0.1264	0.1519
8.5	0.1301	0.1566
9.0	0.1347	0.1613

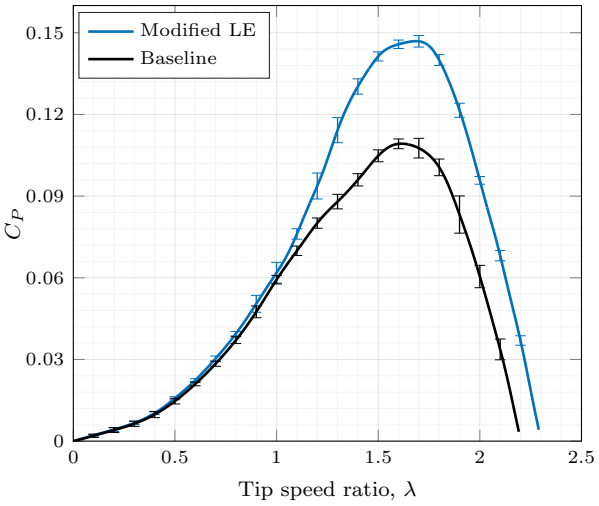

Figure 16: $U_\infty = 7.5\ m/s$.

4. Conclusions

The main objective of the work described in this dissertation was to experimentally evaluate the capability of leading edge protuberances to improve the performance and efficiency of a small vertical axis wind turbine in dynamic stall flow conditions.

The main conclusions of this study are:

1. Even though the finite blade simulation predicted performance values consistent with the experimental data, a very significant sensitivity to the turbulence models and y^+ values was observed. Further dependency analyses would be required to draw final performance conclusions only from the numerical results.

2. The infinite blade simulations' mesh was not

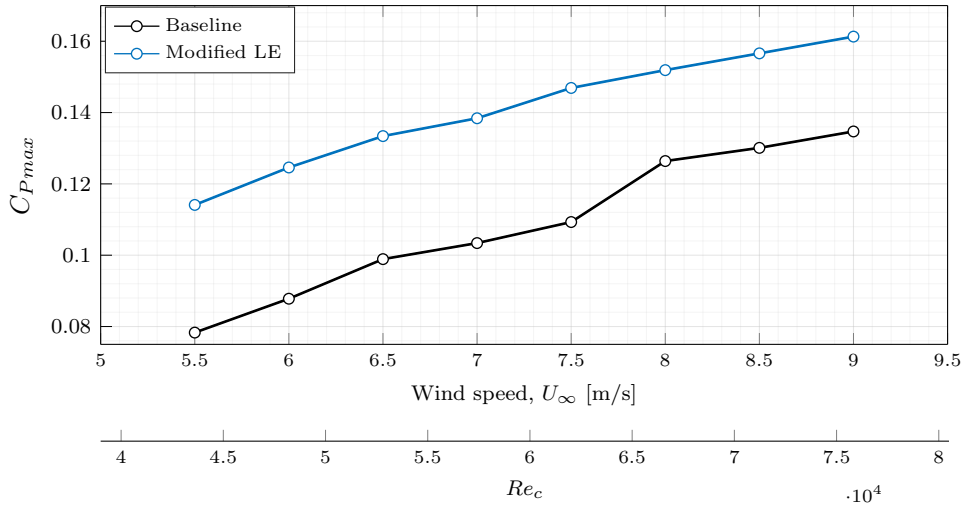

Figure 17: Maximum power coefficient comparison.

capable of predicting the full performance improvements of the modified blades measured in the wind tunnel, possibly due to the lack of blade supports, the tip vortices interactions, and other three-dimensional effects. Even so, the parametric study made with this mesh produced a significantly improved geometry.

3. The experimental setup, developed especially for this study, proved adequate for the suitable evaluation of the turbine's performance in the wind tunnel.

4. The baseline turbine displayed a relatively low maximum power coefficient, C_P, although in the expected range for a turbine of this dimensions and operating in this conditions.

5. The modified blade geometry tested experimentally ($\lambda_{vg} = 1/6c$; $A_{vg} = 0.008c$) markedly enhanced the start-up performance of the turbine in all wind speeds ($U_\infty = 5.5 - 9\ m/s$). The wind speed at which the turbine fails to start was reduced from $U_\infty = 7\ m/s$ to $U_\infty = 5.5\ m/s$ and the time to reach the maximum rotational speed was essentially reduced by half.

6. Similarly, the leading edge protuberances significantly increased the power output/efficiency of the turbine throughout the whole analysed wind speed spectrum. Between $U_\infty = 5.5\ m/s$ and $U_\infty = 6.5\ m/s$ the modified turbine displayed better performance in the entire tip speed ratio range, with around 40% higher peak C_P values. Above $U_\infty = 7m/s$, the performance gains were in general only noticeable above $\lambda > 1$, where the improvement of the maximum C_P fell from 34% to 20%, as the wind speed was increased until 9 m/s.

7. The experimental performance results also showed that the leading edge protuberances did not have a significant effect on the tip speed ratio behaviour.

References

[1] C. Simao Ferreira, K. Dixon, *et al.*, "VAWT in Skew: Stereo-PIV and Vortex Modeling," in *47th AIAA Aerospace Sciences Meeting including The New Horizons Forum and Aerospace Exposition*, American Institute of Aeronautics and Astronautics, 2009.

[2] S. Mertens, *Wind energy in the built environment: concentrator effects of buildings*. Multi-Science, 2006.

[3] E. Möllerström, F. Ottermo, *et al.*, "Turbulence influence on wind energy extraction for a medium size vertical axis wind turbine," *Wind Energy*, vol. 19, no. 11, pp. 1963–1973, 2016.

[4] A. Laneville and P. Vittecoq, "Dynamic Stall: The Case of the Vertical Axis Wind Turbine," *Journal of Solar Energy Engineering*, vol. 108, pp. 140–145, May 1986.

[5] J. L. McCloud III, L. P. Hall, *et al.*, "Full-scale wind-tunel tests of blowing boundary layers control applied to a helicopter rotor," National Aeronautics and Space Administration, Tech. Rep., 1960.

[6] M. A. Karim and M. Acharya, "Suppression of dynamic-stall vortices over pitching airfoils by leading-edge suction," *AIAA Journal*, vol. 32, no. 8, pp. 1647–1655, 1994.

[7] J. C. Magill and K. R. Mcmanus, "Control of Dynamic Stall using Pulsed Vortex Generator Jets," American Institute of Aeronautis and Astronautics, Tech. Rep., 1997.

[8] R. Firdaus, T. Kiwata, *et al.*, "Numerical and experimental studies of a small vertical-axis wind turbine with variable-pitch straight blades," *Journal of Fluid Science and Technology*, vol. 10, no. 1, 2015.

[9] W. Joo, B.-S. Lee, *et al.*, "Combining Passive Control Method for Dynamic Stall Control," *Journal of Aircraft*, vol. 43, no. 4, pp. 1120–1128, Jul. 2006.

[10] L. W. Carr, K. W. Mcalister, *et al.*, "The Effect of a Leading-Edge Slat on the Dynamic Stall of an Oscillating Airfoil," in *AIAA Aircraft Design, Systems and Technology Meeting*, 1983.

[11] D. Baldacchino, C. Ferreira, *et al.*, "Experimental parameter study for passive vortex generators on a 30% thick airfoil," *Wind Energy*, vol. 21, no. 9, pp. 745–765, Sep. 2018.

[12] C. Zhu, J. Chen, *et al.*, "Dynamic stall control of the wind turbine airfoil via single-row and double-row passive vortex generators," *Energy*, vol. 189, Dec. 2019.

[13] C. Zhu, T. Wang, *et al.*, "Numerical Investigation of Passive Vortex Generators on a Wind Turbine Airfoil Undergoing Pitch Oscillations," *Energies*, vol. 12, no. 4, Feb. 2019.

[14] D. De Tavernier, C. Ferreira, *et al.*, "Controlling dynamic stall using vortex generators on a wind turbine airfoil," *Renewable Energy*, vol. 172, pp. 1194–1211, Jul. 2021.

[15] D. S. Miklosovic, M. M. Murray, *et al.*, "Leading-edge tubercles delay stall on humpback whale (Megaptera novaeangliae) flippers," *Physics of Fluids*, vol. 16, no. 5, p. L39, May 2004.

[16] F. E. Fish, P. W. Weber, *et al.*, "The Tubercles on Humpback Whales' Flippers: Application of Bio-Inspired Technology," *Integrative and Comparative Biology*, vol. 51, no. 1, pp. 203–213, Jul. 2011.

[17] J. T. Hrynuk and D. G. Bohl, "The effects of leading-edge tubercles on dynamic stall," *Journal of Fluid Mechanics*, vol. 893, A5, Jun. 2020.

[18] J. Camara and J. Melo De Sousa, "Numerical Study on the Use of a Sinusoidal Leading Edge for Passive Stall Control at Low Reynolds Number," in *51st AIAA Aerospace Sciences Meeting including the New Horizons Forum and Aerospace Exposition*, American Institute of Aeronautics and Astronautics, 2013.

[19] J. L. E. Guerreiro and J. M. M. Sousa, "Low-Reynolds-Number Effects in Passive Stall Control Using Sinusoidal Leading Edges," *AIAA Journal*, vol. 50, no. 2, pp. 461–469, Feb. 2012.

[20] N. Rostamzadeh, K. L. Hansen, *et al.*, "The formation mechanism and impact of streamwise vortices on NACA 0021 airfoil's performance with undulating leading edge modification," *Physics of Fluids*, vol. 26, no. 10, p. 107 101, Oct. 2014.

[21] H. Johari, C. Henoch, *et al.*, "Effects of Leading-Edge Protuberances on Airfoil Performance," *AIAA Journal*, vol. 45, no. 11, pp. 2634–2642, Nov. 2007.

[22] Z. Wang and M. Zhuang, "Leading-edge serrations for performance improvement on a vertical-axis wind turbine at low tip-speed-ratios," *Applied Energy*, vol. 208, pp. 1184–1197, Dec. 2017.

[23] Z. Wang, Y. Wang, *et al.*, "Improvement of the aerodynamic performance of vertical axis wind turbines with leading-edge serrations and helical blades using CFD and Taguchi method," *Energy Conversion and Management*, vol. 177, pp. 107–121, Dec. 2018.

[24] Y. Yan, E. Avital, *et al.*, "Aerodynamic performance improvements of a vertical axis wind turbine by leading-edge protuberance," *Journal of Wind Engineering and Industrial Aerodynamics*, vol. 211, p. 104 535, Apr. 2021.

[25] L. Du, "Numerical and Experimental Investigations of Darrieus Wind Turbine Start-up and Operation," Ph.D. dissertation, Durham University, 2016.

[26] Siemens Digital Industries Software, *Simcenter STAR-CCM+ User Guide, version 2020.2*. 2020.

[27] A. Rezaeiha, I. Kalkman, *et al.*, "CFD simulation of a vertical axis wind turbine operating at a moderate tip speed ratio: Guidelines for minimum domain size and azimuthal increment," *Renewable Energy*, vol. 107, pp. 373–385, Jul. 2017.

[28] Z. Yi-Nan, C. Hui-Jing, *et al.*, "A calculation method for modeling the flow characteristics of the wind turbine airfoil with leading-edge protuberances," *Journal of Wind Engineering and Industrial Aerodynamics*, vol. 212, May 2021.

[29] H. W. Coleman and W. G. Steele, *Experimentation, Validation, and Uncertainty Analysis for Engineers*, 4th ed. John Wiley & Sons, 2018.